Jordan Journal of Civil Engineering, Volume **17**, No. **2**, **2023**
DOI: https://doi.org/10.14525/JJCE.v17i2.13

Single and Ternary Removal of Heavy Metals from Aqueous Solution Using Fe_3O_4 Magnetic Nano-particles

Kamel K. Al-Zboon [1)*]

[1)] Water and Environmental Engineering Department, Huson University College, Al-Balqa Applied University, Irbid, Jordan. * Corresponding Author. E-Mail: alzboon@bau.edu.jo

ABSTRACT

This research aims to investigate the use of magnetic iron nano-particles (FeN) for the removal of heavy metals under single and ternary scenarios. The methodology includes synthesis of FeN using chemical precipitation approach, batch experiments for single and ternary metals removal, isotherm and kinetic studies, thermos-dynamic study and assessing the effect of different parameters on the adsorption process. The results showed that the maximum removal for As and Hg was achieved at a pH of 7, while a pH of 6 provided a slightly higher removal of Cd than a pH of 7 at an optimum mixing time of 120 minutes. The optimum adsorption capacities of As, Cd and Hg at the initial concentration of 200 ppm were 260, 280 and 75.0 mg/g in the case of single metal removal against 91.5, 237.8 and 341.5 mg/g in the case of ternary combination, respectively. The removal of all metals increased with increasing the FeN dose and the mixing time, while it decreased with the increase of the initial concentration. The removal efficiency was affected strongly by the presence of multiple metals, while As removal decreased sharply and Hg removal increased significantly. Adsorption selectivity is affected negatively by the increase in atomic weight and atomic radius. In the case of single-metal removal, fitting of isotherm models can be ranked as Langmuir>Freundlich>Temkin>D-R for As and Cd and Temkin>Freundlich>D-R>Langmuir for Hg, while contradictory results were obtained in the case of ternary combination. Kinetic studies found that the adsorption follows the pseudo-second-order model with R^2=0.99. For all metals, the adsorption process is highly favourable at higher temperatures and is endothermic in nature with (ΔH_o) of 10.91, 23.86 and 0.163 for As, Cd and Hg, respectively. Coating of FeN with silica resulted in lower removal efficiency for all metals up to 50%. It can be concluded that FeN can be successfully used for the removal of heavy metals either through the single or ternary approach, but the single approach provides a higher performance.

KEYWORDS: Nano-materials, Magnetite iron, Adsorption, Arsenic, Cadmium, Mercury, Lead.

INTRODUCTION

Heavy metals are considered among the most toxic substances in water that pose a serious hazard to human health and the environment. Since ions of heavy metals dissolve in water, they can reach the food chain through irrigation, endangering human health and the ecology. The health impact of heavy metals depends on the metal toxicity, the concentration of the metal and the sensitivity of the receptor. The health risks include, but are not limited to, throat constriction, intestinal pain, muscle cramps, cardiac arrhythmias, brain damage and cancer. At high concentrations, some metals may cause immediate death (Alzboon, 2020; Jaishankar et al., 2014).

There are many methods and techniques that have been used to remove heavy metals from contaminated water, such as chemical precipitation, adsorption, ion exchange, biological treatment and membrane separation (Elouear et al., 2008). Due to its high removal efficiency and feasible cost, adsorption is considered one of the attractive methods for heavy-metal removal (Crini, 2005). The removal efficiency of conventional adsorbents depends strongly on the surface area of the adsorbent, its chemical characteristics, pH, metals' selectivity, organic

Received on 10/6/2022.
Accepted for Publication on 29/11/2022.

content, dissolved oxygen content and the adsorption kinetics (Bany Yaseen and Al-Hawari, 2015). Moreover, high removal efficiency needs a high dosage of adsorbent and a long contact time and entails the risk of metals' redissolution and stabilization. For these reasons, the conventional adsorption process is costly and the performance is not guaranteed.

The utilization of nano-materials for water treatment has attracted a considerable attention due to their superior properties. The small size of nano-particles provides a substantially high surface area, which offers a high number of pores on the materials' media, leading to a high ion capacity and subsequently increasing the removal efficiency. In addition, nano-particles have excellent magnetic properties, a high bio-compatibility and a good ability of surface modification. These properties endorse nano-particles to become an attractive option to remove heavy metals from water and wastewater. Alzboon (2017) utilized activated carbon–nano-particle composite for phosphate removal. The results obtained showed that the use of silica nano-particles increased the removal efficiency of activated carbon from 79.9% to 98% at 15wt % of nano-silica. The isotherm study indicated that the adsorption process followed Langmuir and Redlich-Peterson models with high R^2 up to 0.98. High dosage of nano-particles, longer contact time and high temperature caused an increase in the removal efficiency, which, however, decreased with an increase in the initial concentration of phosphate. Dargahi et al. (2016) utilized magnesium oxide nano-particles (MONs) to remove Pb and Cr from contaminated water. They found that the maximum removal efficiency of MONs for Pb and Cr at the initial concentration of 10 mg/L and the adsorbent dose of 0.8 g/l was achieved at pH=9 after a contact time of 280 minutes. Additionally, they found that MONs converted the Pb^{2+} into Pb^0 and Cr^{6+} into Cr^{3+} through the removal process. The adsorption of both metals followed the Langmuir isotherm model. Gayatri et al. (2018) investigated the removal efficiency of Pb on magnetite nano-particles. The maximum adsorption capacity of magnetite nano-particles at 2500 ppm concentration of metal was 62.19 mg/g. It was found that the concentration of the metal adsorbed onto the surface of the nano-particles increased with the increase in the initial concentration of the metal ions and the contact time between the metal and the adsorbent. Meng et al. (2018) prepared magnetic meso-porous silica nano-particles (MSNs), containing iron nano-particles (Fe_3O_4) as the core and a meso-porous silica shell. Amino-groups have been used to modify the characteristics of the prepared shell and to improve its efficiency for heavy metals' removal. The modified adsorbent provided high adsorption of Fe^{+3} that reached 20.66 mg/g. Silver nano-particles (AgNPs) were used to improve the adsorption capacity of bio-adsorbents for heavy metals' removal (Khaled et al., 2018). The results obtained showed that water samples treated with modified bio-adsorbents (sawdust with rice husk) had a better performance in terms of Pb, Cr, NH_3 and NO_2 removal in comparison with non-modified adsorbents. Sodium hypochlorite was successfully used to modify starch nano-particles' adsorption capacity for heavy metals' (Pb^{2+} and Cu^{2+}) removal. The modified nano-particles' material provided high adsorption capacities (>95%) for both metals (Liu et al., 2018).

Peng Yuan et al. (2009) carried out batch tests to investigate the adsorption capacity of prepared magnetite nano-particles for Cr removal. They found that pH has a high impact on the adsorption process. The isotherm and kinetic studies showed that the adsorption followed Langmuir, Freundlich and pseudo-second-order models. The adsorption capacity was 15.3 mg/g and 10.6 mg/g for montmorillonite-supported magnetite and unsupported magnetite, respectively. Synthesized magnetite nano-particles (Fe_3O_4) functionalized with three groups (succinic acid, ethylenediamine and 2,3 dimercaptosuccinic acid) showed a perfect removal efficiency (100%) for selected heavy metal ions (Cd^{2+}, Co^{2+}, + Ni^{2+}, Pb^{2+}, Cr^{3+} and Cu^{2+}) at a pH of 8, while lower removal of As^{3T} was achieved (91–97%) for all used functionalized groups (Singh et al., 2011). Giraldo et al. (2013) used ferric nano-particles for the removal of Pb and Mn from contaminated water. The results showed that the adsorption capacity of magnetic nano-particles for Pb (II) was higher than that for other metals and the adsorption capacity of nano-particles was strongly determined by pH, initial metal concentration, contact time and temperature. Ferric nano-particles provided a high adsorption capacity that reached 0.180, 0.170, 0.160 and 0.140 mmol/g for Pb^{2+}, Cu^{2+}, Zn^{2+} and Mn^{2+}, respectively, at the optimum conditions. The adsorption process followed the pseudo-second-order mechanism.

Selected heavy metals have been removed successfully by iron nano-particles (Fe_3O_4) coated with humic acid and the results showed that a high removal efficiency can be achieved by the functionalized Fe_3O_4, reaching up to 99%, 99%, 95% and 95% for Hg^{2+}, Pb^{2+}, Cu^{2+} and Cr^{2+}, respectively. The equilibrium status was achieved after 15 minutes and the adsorption isotherm fitted well with the Langmuir model (Liu et al., 2018). Yantasee et al. (2007) synthesized (Fe_3O_4) nano-particles functionalized with dimercaptosuccinic acid and used them for the adsorption of selected heavy metals. The produced nano-particles had a surface area of 114 m^2/g. The results revealed that 99% removal of low-concentration Pb (1 mg/L) can be achieved within one minute of contact time. The maximum Hg sorption capacity of the modified nano-particles was 227 mg/g.

This research aims to investigate the capability of FeN and FeN-S for heavy metals' removal under single and ternary scenarios. In this work, one batch will be used for the removal of three hazardous metals using a low dose of a single adsorbent. This method provides simultaneous high removal efficiency of many metals by low-cost material, short time and safe approach. To the best of the author's knowledge, similar works and scenarios for the same metals were not reported. In this research, Fe_3O_4 nano-particles will be synthesized chemically in the lab and will be modified by coating with silica nano-particles. The selectivity of Fe_3O_4 nano-particles for heavy metals' removal (Hg, Cd and As) will be investigated under variable environmental conditions, such as pH(4-8), Co (10-200ppm), dose (0.03-0.06 g) and mixing time (10-180 minutes). Isotherm and kinetic behaviours of the adsorption process will be investigated. It is expected to synthesize low-cost nano-particles with a high removal efficiency within a short time and a low dose of adsorbent.

METHODOLOGY

Materials

All chemicals used for synthesizing, coating and functionalizing of FeN and for adsorption experiments were of an analytical grade. For synthesizing of FeN, the analytical grades were: for ferrous chloride tetrahydrate ($FeCl_2.4H_2O$, molar mass: 198.81 g/mol), for ferric chloride hexahydrate ($FeCl_3.6H_2O$, molar mass: 270.33 g/mol), for ethanol (C_2H_5OH, molar mass: 46.07 g/mole) and for acetone (CH_3COCH_3, molar mass: 58.08 g/mole) as obtained from Merck, Germany, while sodium hydroxide (NaOH) from Alphachmika, India was used. To determine the performance of FeN for heavy metals' removal, analytical gradients of $Pb(NO_3)_2$, 99.5%; HgO, 99.5%; As_2SO_3, 99.5%; and $Cd(NO_3)_2.4H_2O$, 99% from SDFCL, India were used for the adsorption experiment. Methylene blue ($C_{16}H_{18}ClN3S$, molecular weight= 319.85) from Merck was used to estimate the surface area. Tetraethyl orthosilicate ($Si(OC_2H_5)_4$, molecular weight= 208.33) from Merck was used as a source of silica coating. Deoxygenated water saturated with N_2 was used to synthesize FeN, while deionized water was used for FeN and FeN-S washing.

Instrumentation

XRD analysis was performed using Ultima IV (185mm) made by Rigaku for both pure FeN and FeN-S nano-particles. Continuous scanning of 2theta with a speed of 3.0 deg/min and a K-Beta filter was carried out. FTIR – Alpha 2 from Bruker was used to determine the functional groups for both samples (FeN and FeN-S). Scanning was conducted in the wavenumber range of 416.97–5000/cm. The particle sizes and distribution were determined by FEI Versa Three-dimensional (3-D) Dual Beam Field SEM (scanning electron microscope) at HV of 30kV, WD of 8.7mm and a spot of 3. Heavy-metal concentrations were determined by Inductively Coupled Plasma Mass Spectrometry (ICP-MS) NexION 2000B from Perkin Elmer.

Synthesizing FeN

FeN was synthesized using the co-precipitation approach as reported by Al Jarrah et al. (2018). NaOH (0.64M) was dissolved in 750 ml of deoxygenated water and was put in the reactor. Solutions of $FeCl_2.4H_2O$ and $FeCl_3.6H_2O$ were prepared individually by dissolving one mole and two moles, respectively, in 100 ml of deoxygenated water. Then, both solutions were mixed using a magnetic stirrer (360 rpm) for about 30 minutes. Iron salts' solutions (Fe_3-Fe_2) were added dropwise to the NaOH solute with vigorous mixing under controlled temperature (70–80°C) for about 2 hours. The pH value was maintained in the range of 11–12 throughout the mixing time. During mixing, the possible interference of

oxygen was eliminated through a continuous nitrogen stream in the reactor. A black precipitate of Fe_3O_4 formed immediately after the addition of (Fe_3-Fe_2) solutions according to Equation (1). After the completion of the reaction, the supernatant water was decanted and filtrated, while the precipitate material was collected by a magnet and washed several times with ethanol and distilled water solution (3:1) to achieve a neutral pH. After collection, the synthesized FeN was dried in an oven at 60°C for 24 hours, after which it was ground and stored in a desiccator for further experiments.

$$FeCl_2 + 2FeCl_3 + 8NaOH \rightarrow Fe_3O_4 + 8NaCl + 4H_2O \quad (1)$$

Synthesizing FeN-S

Coating of FeN with silica has many advantages. It increases the stability of FeN, protects FeN from acid dissolution and reduces the bulk conductivity. Moreover, silica can coat the surface without affecting the chemical redox reaction on FeN surface and reduce the agglomeration of FeN (Roto, 2018).

An amount of about 3 grams of FeN was added to a solution of 50 ml of double-distilled water, 500 ml of ethanol and 10 ml of TEOS and stirred for about one hour. NaOH (50 ml, 10%wt) was added dropwise to the prepared TEOS solution under mixing for about 4 hours. The synthesized FeN-S was precipitated using a magnet, the supernatant water was decanted and filtrated, while the precipitate material was collected by a magnet and washed several times with ethanol and distilled water solution (3:1) to achieve a neutral pH. After collection, the synthesized FeN-S was dried in an oven at 60°C for 24 hours, after which it was ground and stored in a desiccator for further experiments. A similar approach was followed by Al Jarrah et al. (2018).

Determination of Adsorbent's Surface Area

The areas of FeN and FeN-S were determined by using methylene blue as an adsorbate as described by Ahiduzzaman and Islam (2016). Methylene blue concentrations of 50, 100, 200 and 300 ppm were put in the test batch jars and 0.02 g of FeN was added to each batch and mixed for 2 hours at room temperature. After mixing, the decanted water was filtered and analyzed for MB absorption using a spectrophotometer. The standard calibration curve of MB (Figure 1) was used to determine MB concentration based on the absorbance (nm). The specific area was calculated as below (Ahiduzzaman and Islam, 2016):

$A = qm^* N^* 130 Å^2$

where A: the specific area (m^2), qm: adsorption capacity (mole/g), N: Avogadro number, $Å = 10^{-10}$.

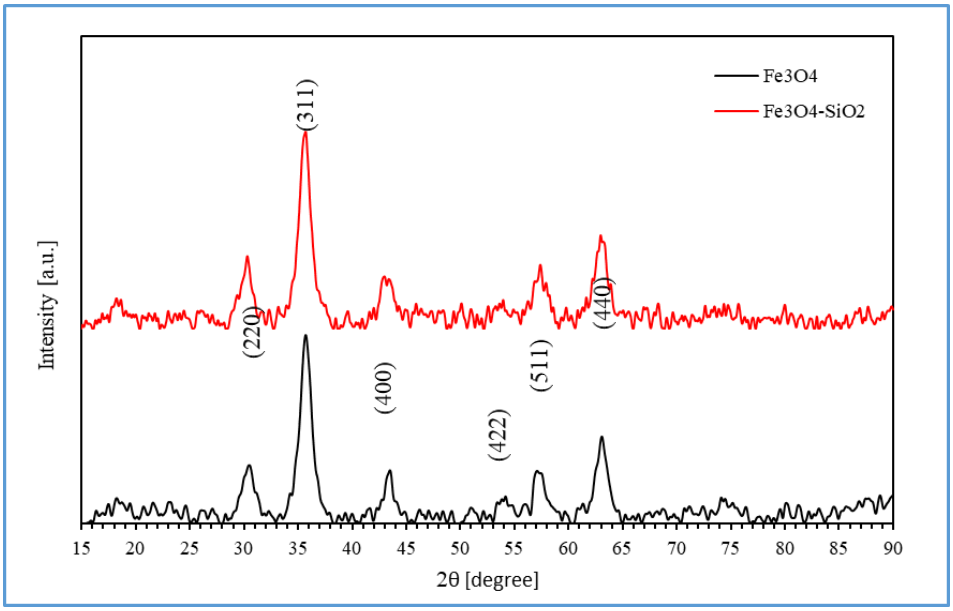

Figure (1): XRD results of FeN and FeN-S

Determination of Particle Size

Average particle size was determined using Scherer's formula (Vorokh, 2018):

Crystallite size Dp= Kλ /(Bcos)

where Dp - Average crystallite size (nm).

K - Scherrer constant (with values of 0.62 to 2.08).

λ - X-ray wavelength. For Mini XRD, Cu Kα average = 1.54178 Å.

B - FWHM (full width at half maximum) intensity of XRD peak.

θ - XRD peak position.

Adsorption Studies

Variable concentrations (50, 100, 150, 200 and 350 ppm) of As, Cd and Hg were prepared by dilution of the stock solution with distilled water. The adsorption tests were performed at different pH (4, 5, 6, 7 and 8), different adsorbent doses (0.03, 0.04, 0.05 and 0.06g), variable mixing times (10, 30, 45, 60, 120 and 180 min.) and three different temperatures (25, 35 and 45 °C). To determine the removal efficiency, the concentrations of the heavy metals were measured before and after the adsorption tests by Inductively Coupled Plasma Mass Spectrometry (ICP-MS) NexION 2000B from Perkin Elmer. The adsorption efficiency and the adsorption capacity were calculated as reported by Alzboon et al. (2016).

Thermo-dynamic Study

Four isotherm models were used in this research; namely, Langmuir, Freundlich, Dubinin–Radushkevich and Temkin models, as shown in Equations (2-5), respectively (Alzboon & Harahshah, 2018).

$$\frac{1}{qe} = \left(\frac{1}{kaqm}\right) * \left(\frac{1}{Ce}\right) + \left(\frac{1}{qm}\right) \quad (2)$$

$$\log(qe) = \log(kf) + \frac{1}{n}\log(ce) \quad (3)$$

$$ln(qe) = ln(qm) - K\ \varepsilon^2) \quad (4)$$

$$qe = B\ ln(At) - B\ lnCe\ ) \quad (5)$$

where qe: is the equilibrium adsorption capacity at a certain concentration Co, qm: is the optimum equilibrium uptake capacity, Ka: is a constant related to the heat of adsorption and Ce: is the remaining concentration. The linear trend of plotting of 1/qe *vs.* 1/Ce results in 1/qm (the constant) and the slope is 1/(ka*qm). Kf, n and k are Freundlich model's coefficients.

ε is the Polanyi potential (kJ mol^{-1}) which can be calculated by Equation 6:

ε = RTln(1+1/Ce) (6)

where R is the universal gas constant (8.314 J mol^{-1} K^{-1}), T is the temperature (K), B is a constant of heat adsorption (J/mol) which can be calculated by Equation (7):

B= RT/bt (7)

where bt: isotherm constant, At in Equation (5): constant of equilibrium binding (l/g).

Kinetic Study

Three kinetic models were used: pseudo-second-order, pseudo-first-order kinetic and intraparticle models. While pseudo-second-order and pseudo-first-order are functions of time, the intraparticle model is a function of half-time (t^0.5). The linear forms of the mentioned models are shown in Equations (8–10), respectively (Alzboon et.al., 2016):

$t/qt=1/k_1q_e^{\ 2} + t/qe$ (8)

$ln(qe-qt)=ln(qe)-k_2t$ (9)

$qt=k_3t^{1/2}+k_4$ (10)

where q_e is the equilibrium adsorption capacity, q_t is the adsorption capacity at time t, k_1, k_2, k_3 and k_4 are constants of the models, respectively, while t is the time in minutes. k_1, k_2 and k_3 values can be obtained by plotting a graph of t/q against t, ln ($q_e - q_t$) against t and q_t against $t^{0.5}$, respectively.

RESULTS AND DISCUSSION

Characterisation of Nano-particles

The XRD pattern showed peaks at 2Θ of 30.8, 35.74, 43.56, 53.78, 57.12 and 63.12° (Fig. 1), which matched the magnetite crystal planes (hkl) of 220, 311, 400, 422, 511 and 400, respectively (Anjaneyulu et al., 2018). This result proved the pure formation of magnetite nano-phase with no hematite or other impurities. Matching of intensity with standard hkl planes indicates that the samples are polycrystalline and have face-centred cubic structures. However, in both cases, the intensities of

(311) were extremely high compared to other diffraction lines, indicating that they are the preferential orientation of the micro-strain (Alzoubi et al., 2021). The increased peak intensities were attributed to grain growth associated with preferred orientation and/or increase in the degree of crystallisation. A comparison of the XRD patterns of FeN and FeN-S showed that there is no difference in the intensity patterns, but a higher peak intensity was found for the FeN-S sample, which may be explained due to the excess amount of silica used in coating (Al-Jarrah et al., 2018).

According to the SEM image, the size of FeN particles ranged from 7.28 to 16.03 nm against a range of 14.77 to 31.78 nm for FeN-S. The larger particle size of FeN-S revealed the formation of successful coating (Fig. 2). While FeN showed a non-uniform distribution of particles and a high agglomeration with complex structure, FeN-S showed a better distribution of particles and less agglomeration with excess particles provided by multi-layers of coating. Most of FeN particles had spherical shape with some particles having elliptical, ellipsoidal, micro ridge and segmental head shapes, while FeN-S particles had mostly a spherical shape. The difference in FeN particle shape is attributed to the manual grinding of particles.

Figure 3 shows the FTIR intensity of the functional groups. It was reported that all magnetite bands are below a wavenumber of 600/cm (Bertolucci et al., 2015). The presence of Fe_3O_4 is shown in a strong band at 542.55/cm. No significant bands were shown in the typical range of hematite phase of 740–620/cm, revealing the successful formation of magnetite and the absence of hematite. A strong band for FeN was noticed at a wavenumber of 2361/cm, indicating a C-H stretching group, while a C-O-O group was found at a wavelength of 1541.1 cm.

For the FeN-S sample, additional functional groups were found related to silica and water. A sharp bending peak was observed at 545 cm matching the typical Fe-O-Si band (Fig. 3). At wavelengths of 800 cm and 1218 cm, bending vibrations of Si-O-Si and Si-O at 990 cm were found, indicating a successful coating of FeN by silica (Roto, 2018). A bending vibration of H-O-H group was found at a wavelength of 1636 cm and a vibrate stretching of OH group was found at wavelengths of 3300 cm and 3763 cm (Malega et al., 2018).

Performance of FeN and FeN-S

Figure 4 shows that FeN has a higher removal efficiency than coated samples for all metals. After coating, the removal efficiency of FeN decreased by 26, 12 and 46% for Hg, Cd and As, respectively. This result can be attributed to the lower surface area of coated FeN-S (64 m^2/g) in comparison with pure FeN (87 m^2/g) due to the larger size of FeN-S. In some cases, silica coating occurs at multi-layers, which reduces the interference between the adsorbent (FeN) and the adsorbates (heavy metals). The adsorption-capacity values of FeN and coated FeN (doses of 0.02 g and Co of 50 mg/l) were 113.75, 107.5 and 105 mg/g and 85, 92.5 and 57.5 mg/g for Hg, Cd and As, respectively. It was reported that surface modification of magnetic nano-particles is useful to prevent aggregation (Manyangadzea et al., 2020). Han et al. (2013) found that the dissolved silicate did not affect the removal of Arsenite by the NP-FeS, while it had a negative impact on the adsorption of As on Fe-hydroxide systems.

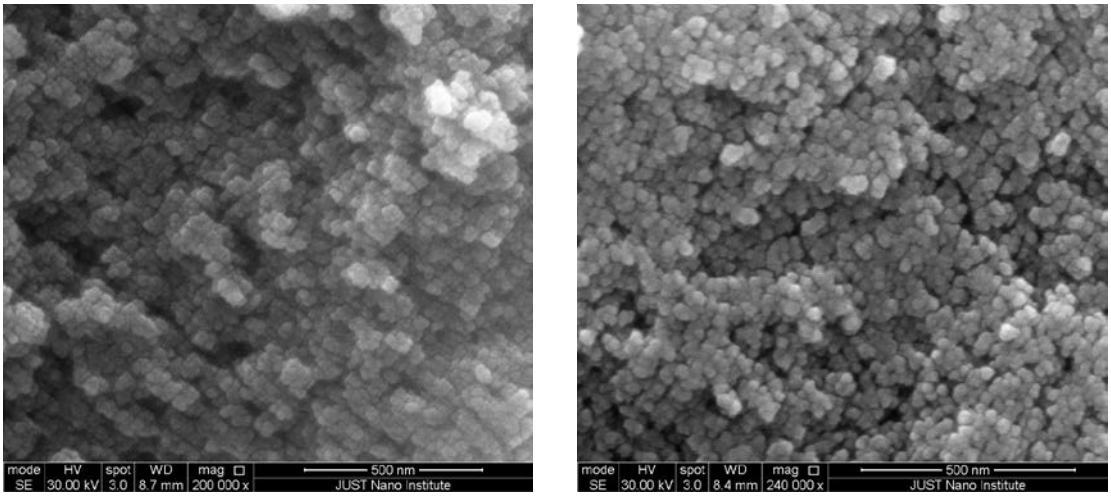

Figure (2): SEM images of FeN (left) and FeN-S (right)

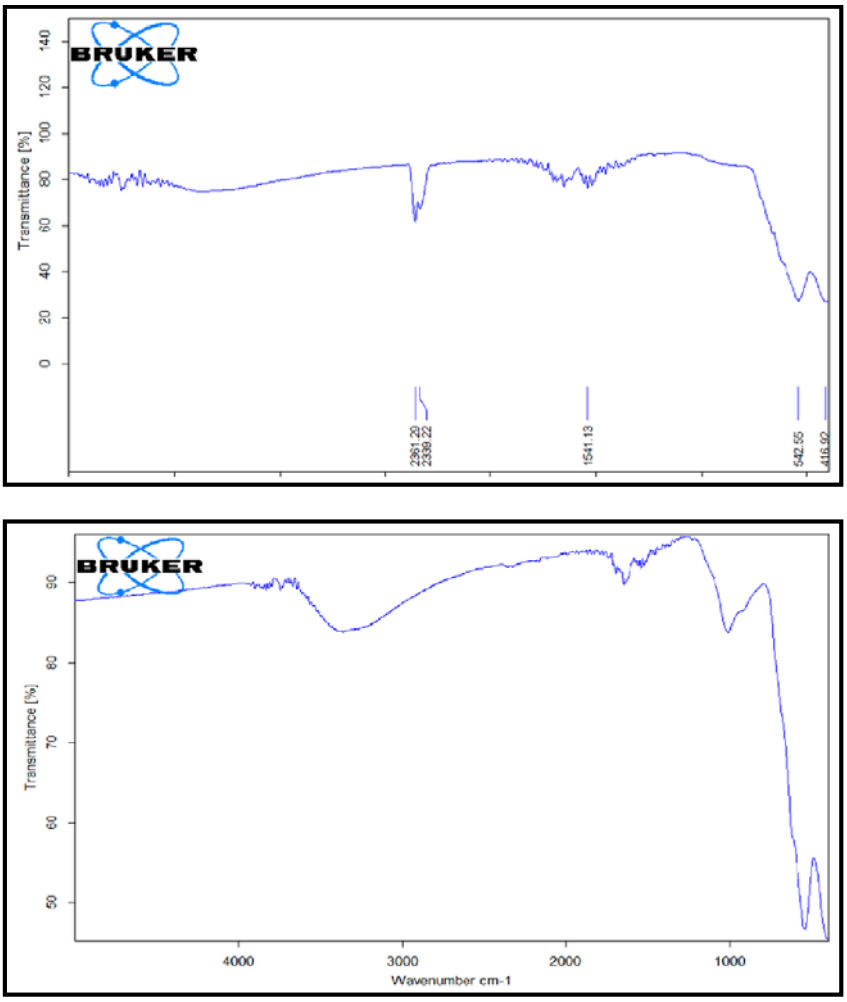

Figure (3): FTIR results of FeN (up) and FeN-S (down)

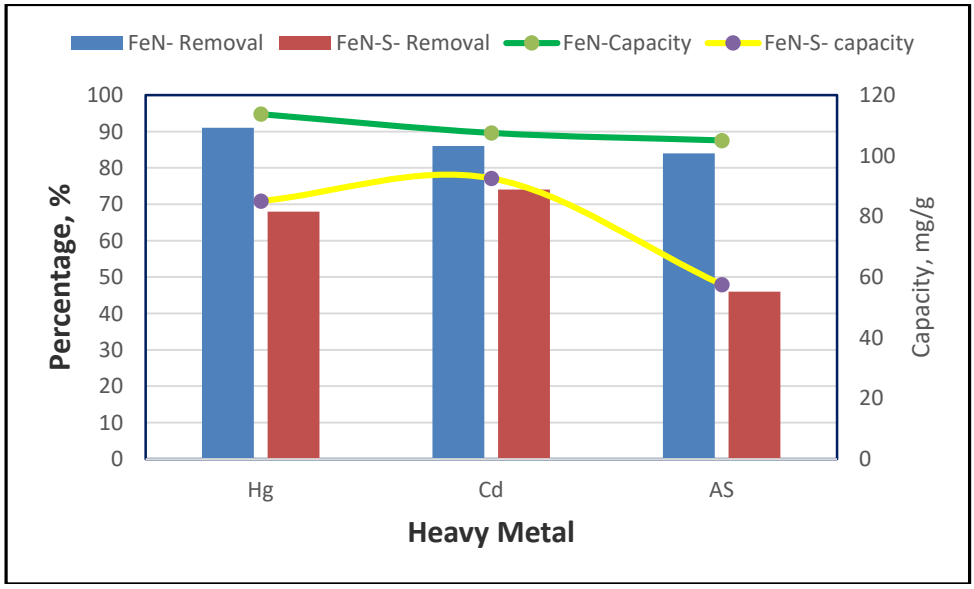

Figure (4): Removal efficiency of FeN and FeN-S

Impact of FeN Dosage

Figure 5 shows that the removal efficiency of As and Cd increased significantly as FeN dose increased, while there was no significant change in the removal efficiency of Hg. As the dose increases, the available pores of the adsorbent increase, providing more active surface area to accommodate the adsorbate, which enhances the removal efficiency of the metals. There was a non-linear increase in the removal efficiency of As and Cd from 65.8% and 67.9% at a dose of 0.03 g to 77.0% and 75.40 at a dose of 0.06 g for both metals, respectively. Hg removal increased from 98 to 99% for the respective doses. The removal capacity decreased as the dose increased, indicating that the additional amount of adsorbent did not have the same performance as the previous one; this can be attributed to the high competition of metals on the available pores at the low dose of adsorbent. The removal capacity of As, Cd and Hg decreased from 54.83, 56.6 and 84.8 mg/g at a dose of 0.03 to 32.0, 31.4 and 41.1 mg/g at a dose of 0.06 g for the considered metals, respectively. This result is in line with those obtained previously (Alzboon, 2017; Alzboon & Al-Harahsheh, 2019).

Impact of pH

For As and Hg, higher removal efficiency was achieved at a pH of 7, while a pH of 6 provided a slightly higher removal of Cd than a pH of 7 (95.4% against 94.5%). For this reason, a pH of 7 was considered as the optimum one and was selected to be used for further experiments. Removal efficiency of As, Cd and Hg increased from 75%, 45.8% and 91.5% at a pH of 4 to 85%, 94.5% and 96.8% at a pH of 7 for the considered parameters, respectively. Similarly, the maximum adsorption capacity was achieved at pH values 6-7 and reached 106.5, 119.2 and 120.9 mg/g for As, Cd and Hg, respectively (Fig. 6). It was observed that Cd had a higher sensitivity to pH variation than the other two metals.

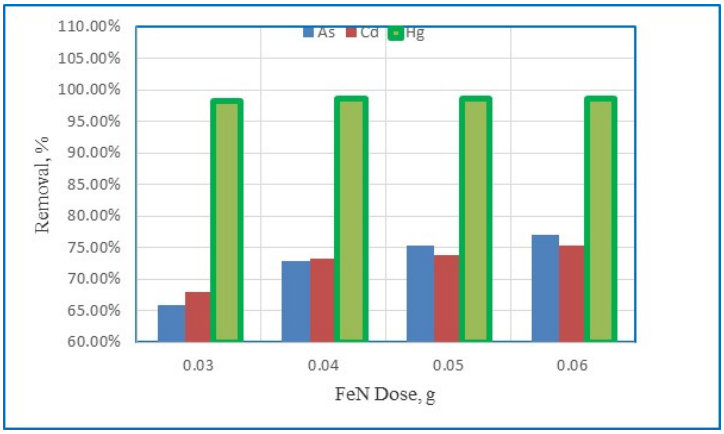

Figure (5): Effect of FeN dosage on the removal of As, Cd and Hg

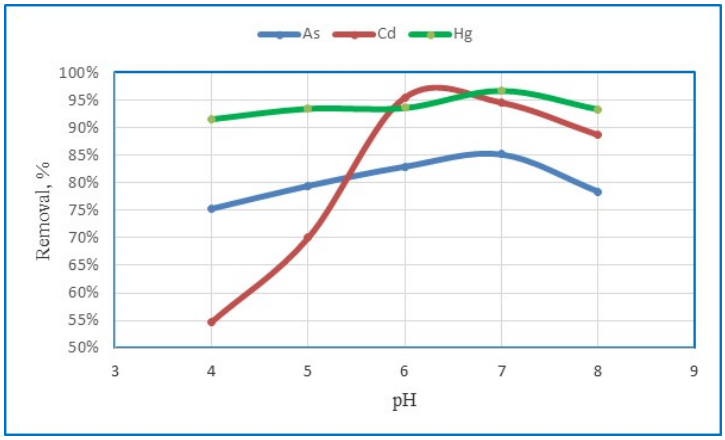

Figure (6): Effect of pH on the removal of As, Cd and Hg

The pH value has a high impact on the nature of the adsorbent surface as well as the type of adsorbate distribution. At a low pH, the net interaction in the solution is electro-static repulsion due to the positive charge of both adsorbent surface and adsorbate species (H^+ and M^{2+}, respectively). Additionally, at a low pH, the high concentration of H^+ in the solution creates a high competition between H^+ and the positively charged metal ions to fill the available pores on the adsorbent surface (Goel et al., 2004). At a higher pH, the concentration of H^+ decreases, resulting in less competition between H^+ and the metal ions; subsequently, all pores become available to accommodate metal ions.

Fato et al. (2019) found that ultrafine Fe_3O_4 nano-particles provided the highest removal of Pb^{2+}, Cd^{2+}, Cu2+ and Ni^{2+} at a pH of 6 and remained constant beyond that. Xiaotao et al. (2016) reported that the optimum pH for removal of Cd(II) and Hg(II) ions on synthesized activated carbon was observed at 5.1 and 4.5, respectively.

Impact of Initial Concentration on Single and Ternary Metals' Adsorption Systems

The effect of initial concentration on the adsorption of a single metal was performed at five different concentrations (50, 100, 150, 200 and 350 ppm). For all metals, the removal efficiency decreased with the initial concentration increase. In contrast, the adsorption capacity increased significantly with the initial concentration increase. At a low concentration (50 mg/l), a removal efficiency of 60–70% was achieved for the three metals; however, different results were obtained at a higher concentration (350 mg/l), where As and Cd achieved good removal-efficiency values (50% and 47%). However, the removal efficiency of Hg decreased to 11%. This result may be attributed to the low atomic weight of As (74.92) in comparison with the atomic weights of Cd (112.4) and Hg (200.59). This indicates a strong relationship between adsorption and atomic weight. Also, Hg has a larger atomic radius (171pm) in comparison with Cd (161 pm) and As (114 pm), which is considered an additional factor affecting the adsorption process.

To determine the impact of high concentration on the removal efficiency and the removal capacity of FeN in a ternary system, six different concentrations of As, Cd and Hg (10, 20, 30, 50, 100 and 200 mg/l) were simultaneously applied to the solution. In this approach, concentrations lower than the single adsorption system were applied as high competition between the metals was expected. Fig. 7 shows that the removal efficiency decreased significantly as the initial concentration increased for all metals. The maximum reduction in the removal efficiency was observed for As (72%), followed by Cd (41%), while Hg had the lowest reduction (30%). In contrast, the removal capacity increased sharply as the initial concentration increased from 50 to 200 ppm and reached 4.5, 10.9 and 13 times for As, Cd and Hg, respectively. At high concentrations of metals, the available pores of FeN become insufficient to accommodate all metal ions and some of them are not absorbed and remain in the solution. The competition between metals appeared clearly at high concentrations; while Hg was slightly affected with the increase of the initial concentration, As was sharply affected. In the single system, all pores are available for a single metal, while there is a high competition between metals in case of the ternary system and the available pores become insufficient to adsorb all metals. Sobhanardakani et al. (2015) found that in a binary adsorption system of Cd and Hg on chitosan, both metals had high removal-efficiency values at low concentrations, while at high concentrations, Cd had a higher removal efficiency than Hg.

Competition of Metals in a Ternary System

Table 1 shows the impact of the ternary system on the removal efficiency and adsorption capacity of metals. Clearly, the ternary system has an insignificant effect on Cd removal at Co of 50 and 100 ppm. In contrast, As and Hg are notably affected. While As removal sharply decreased, Hg removal increased significantly. Hg and As were affected significantly even at low concentrations and the influence of the ternary system increased with initial concentration increase. It can be concluded that in the case of the ternary system, Hg was adsorbed preferentially and most of the pores were occupied by Hg and Cd. The adsorption selectivity can be ranked as: Hg >Cd >As. Similarly, Xiaotao et al. (2016) reported that Cd removal was not affected due to the presence of Hg in the binary system, while Hg was affected significantly. Dias et al. (2021) found that the absorptivity of metals by hazelnut,

peanut and walnut can be ranked as: Cd>Pb>Hg. Additionally, they found that the transition from single to ternary adsorption system resulted in a decrease in Hg and Cd removal by 14% and 7%, respectively, while Pb showed an insignificant change.

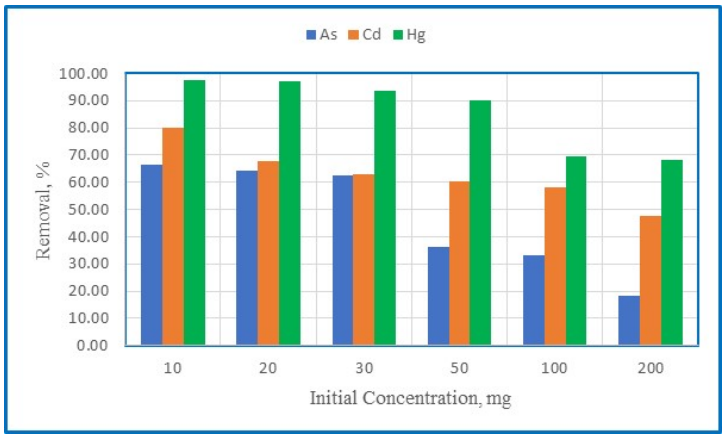

Figure (7): Effect of the initial concentration of FeN dosage on the removal of As, Cd and Hg through ternary system

Table 1. Removal efficiency of single and ternary adsorption systems

Initial concentration mg/l	Metal	Removal efficiency, %		Adsorption capacity, mg/g	
		Single system	Ternary system	Single system	Ternary system
50	AS	66	36.1	82.5	45.1
	Cd	60	60.3	75.0	75.3
	Hg	70	90.3	87.5	112.9
100	AS	61	33	152.5	82.5
	Cd	59	58.3	147.5	145.8
	Hg	40	69.7	100.2	174.3
200	As	52	18.3	260	91.6
	Cd	56	47.6	280.1	237.9
	Hg	15	68.3	75.0	341.5

Impact of Mixing Time

Figure 8 shows the impact of mixing time on the removal efficiency of FeN. It is seen that the removal efficiency increased with the increase of mixing time during the studied period (3 h). While a significant increase was noticed during the first hour, only a slight increase occurred beyond that. Longer time increases the contact period between the adsorbent and the metals, subsequently increasing the opportunity for removal. After 10 minutes of mixing, we can achieve removals of 81%, 71% and 80% for As, Cd and Hg, respectively. A mixing time of 30 minutes can provide more than 84% of the final removal for all metals, indicating the feasibility of using a shorter time which will save time and cost. Many researchers reported a high feasible removal efficiency after 30 minutes (Alzboon et al., 2017; Sobhanardakani et al., 2015).

Isotherm Study of Single Metal Adsorption

The result of using the four isotherm models for single metal adsorption is shown in Table 2. It is seen that the Langmuir model showed the best fit for As, Cd and Pb, while the Temkin model showed the highest R^2 value for Hg. Based on R^2, the models' fitting can be ranked as: Langmuir>Freundlich>Temkin>D-R for As, Cd and Pb and Temkin>Freundlich>D-R>Langmuir for Hg. The high fitting of adsorption process to the Langmuir model indicates that a mono-layer adsorption is predominant. The maximum adsorption capacity of the Langmuir model (qm) for As, Cd and Pb was more

than the equilibrium capacity (qt) at the initial concentration of 350 ppm, indicating the availability of unoccupied pores and an opportunity for additional metal removal. For Hg, all models showed low R^2, which indicates that other removal processes rather than adsorption may have occurred. The Freundlich model showed that n values ranged from 1.29-6.93, indicating a favourable sorption process (Dada et al., 2012). Very low values of ε (<4 kJ mol^{-1}) of the D-R model for all metal ions indicated a physical adsorption process (Fato et al., 2019).

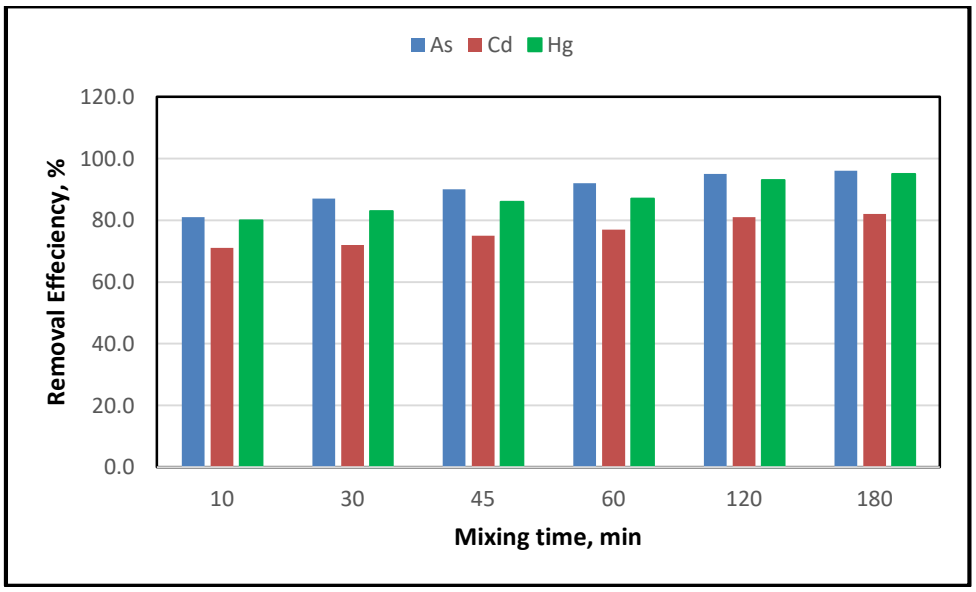

Figure (8): Effect of mixing time on the removal of As, Cd and Hg

Table 2. Results of isotherm models for single adsorption

Metal	Indicator	Langmuir	Freundlich	D-R	Temkin
As	R^2	0.993	0.99	0.74	0.91
		qm = 555.56	Kf = 11.32	qm = 276.77	B = -144.83
		Ka = 0.01	n = 1.42	K= -0.00006	At = 12.8816
Cd	R^2	0.99	0.98	0.83	0.97
		qm = 1111.11	Kf = 7.97	qm = 288.99	B = -153.04
		Ka = 0.0036	n= 1.29	K= -0.0001	At = 14.127
Pb	R^2	0.91	0.90	0.611	0.75
		qm=285.71	Kf=47.64	qm= 251.92	B= -80.92
		Ka= 0.077	n= 2.65	K=0.000009	At= 2.88
Hg	R^2	0.126	0.243	0.128	0.302
		qm=112.36	Kf=56.49	qm= 114.15	B= -19.237
		Ka= 0.22	n= 6.93	K=0.00001	At= 0.247

The dimensionless separation factor (RL) is used as an indicator of adsorption favourability. It can be calculated as shown in Equation below. It was reported that if 0<RL<1, it indicates a highly favourable adsorption process (Alzboon & Harahshah, 2019; Dada et al., 2012). The values of RL were: 0.026, 0.44 and 0.22 for Hg, Cd and As, respectively. Since RL values are close to zero, this indicates an irreversible adsorption process.

$RL= 1/(1+KaC_o)$,

where *Ka* is the Langmuir adsorption constant and C_0 is the maximum initial concentration.

Isotherm Study of Ternary Metal Adsorption

The Langmuir model showed the best fit for As and Hg, while the Freundlich model was the best fitting model to Cd. In comparison with the single metal isotherm, As and Cd showed low values of Langmuir qm, while Hg showed a higher value (Table 3). The percentage of qm/qt at an initial concentration of 350 ppm reached 48%, 50% and 100% for Hg, Cd and As, respectively, against 64.2%, 270% and 127% in the case of single metal removal. Langmuir and Freundlich models showed a good correlation for Hg adsorption, while all models showed an insignificant correlation for mono-adsorption of Hg. The model significance can be ranked as: Langmuir > Freundlich>Temkin > D-R for As, Freundlich > Langmuir > Temkin > D-R for Cd and Langmuir > Freundlich > Temkin > D-R for Hg. RL values were 0.0072, 0.051 and 0.075 for Hg, Cd and As, respectively, where a low value of RL meant an irreversible adsorption in nature. Sobhanardakani et al. (2015) found that both models (Langmuir and Freundlich) provided a high correlation ($R^2 > 0.97$) for Cd and Hg.

Table 3. Results of the isotherm models for ternary adsorption

Metal	Indicator	Langmuir	Freundlich	D-R	Temkin
As	R^2	0.978	0.90	0.78	0.965
		qm = 99.0	Kf = 13.11	qm = 62.96	B = -19.70
		Ka = 0.062	n = 2.42	K = 0.000003	At = 1.391
Cd	R^2	0.915	0.98	0.5	0.883
		qm = 120.48	Kf = 11.41	qm = 92.16	B = -56.5
		Ka = 0.093	n = 1.52	K= 0.000002	At = 2.76
Hg	R^2	0.975	0.97	0.70	0.835
		qm = 163.93	Kf = 51.60	qm = 146.27	B = -49.16
		Ka= 0.693	n = 2.34	K=0.0000007	At = 0.274

Kinetic Study

Three kinetic models (pseudo-first-order, pseudo-second-order and intraparticle) were applied to investigate the adsorption behaviour along the time (Table 4). The result shows that the second-order model is the most suitable one for all metals, while the intraparticle model is the lowest fitting one. High fitting of the second-order model indicates that the adsorption is not only a physical process in nature. Intraparticle model assumed that adsorption occurs due to film diffusion (interference in the solution) and then the intraparticle diffusion brings the adsorbate to the pores of the adsorbent particles (Al Hamouz & Ali, 2013). Good agreement of the intraparticle model with adsorption results (R^2>0.89) reveals that the diffusion phenomenon has a significant effect on the adsorption process. For an initial period of reaction (time<30min), both models (pseudo-first-order model and intraparticle model) provided good fitting to the data, while the second-order model provided good agreement for most of time. Intraparticle model suggested that the adsorption process consists of three stages: the first one shows the external diffusion lasting from 0 to 10 minutes with a sharp increase in metals' removal and adsorption capacity, the second stage is a linear line with a medium slope that shows the intra-diffusion process lasting from 10 to 120 minutes and the third stage shows the near-equilibrium low-diffusion process due to limited concentrations of metals lasting from 120 to 180 minutes (Al Jarrah et al., 2018).

Table 4. Results of the kinetic models

Parameter	1st order	2nd order	Intraparticle
As	0.94	0.99	0.89
Cd	0.94	0.99	0.95
Hg	0.93	0.99	0.98

Thermodynamic Study

Thermo-dynamic study is very important to describe the nature of the adsorption process. Thermo-dynamic experiments were carried out at three temperatures (25, 35 and 45°C) with a constant pH (7), an initial concentration (50 ppm), a mixing time (120 min) and an FeN dose of 0.02 g.

Thermo-dynamic indicators, entropy (ΔS_o, kJ/mol)

and enthalpy (ΔH_o, kJ/mol), can be determined by plotting the LnKd against 1/T, where the slope represents $\Delta H_o/R$, while the intersect represents $\Delta So/R$, as shown in the following Equation (Alzboon et al., 2017):

$\ln Kd=(\Delta So/R) -- (\Delta Ho/RT)$

where Kd is the partition coefficient and is used as a measure o the adsorption process. It is calculated as shown in the following equation (Alzboon et al., 2016):

$Kd = (Co-Ce)XV/(Co\times m)\times 100\%$.

The change in Gibbs free energy ($\Delta G°$, kJ/mol) was calculated as follows:

$\Delta Go=\Delta Ho- T\Delta So$.

The value of Kd increased with temperature increase; i.e., from 1.32, 1.30 and 2.40 at 25°C to 1.75, 2.37 and 2.41 at 45°C for As, Cd and Hg, respectively, indicating that the adsorption process is highly favourable at higher temperatures and is endothermic in nature. (Alzboon & Al Harahsheh, 2019).

The values of enthalpy (ΔH_o) were 10.91, 23.86 and 0.163 for As, Cd and Hg, respectively. The positive values of ΔH_o for all metals indicate an endothermic process. It was reported that the chemisorption process occurs at ΔHo value range of 80-200 kJ/mol, since at ΔH_o values less than this range, the adsorption is a physisorption process (Saha & Chowdhury, 2011). ΔSo values were 0.038, 0.083 and 0.0078 kJ/mol for As, Cd and Hg, respectively. Since ΔH values were more than TΔS0, the adsorption process is mostly an entropy-controlled process (Sismanoglu et al., 2004). The high entropy of As and Cd can be attributed to the separation of hydrated-water molecules from metal ions before they attach to the FeN surface or enter inside the adsorbent matrix, which increases the heterogeneity of the adsorption process and subsequently increases the entropy (Donat et al., 2005).

The values of ΔG° at T=25°C were -0.656, -0.898 and -2.18 for As, Cd and Hg, respectively and decreased with increase in temperature. While Hg had the lowest ΔG°, As had the highest at all temperatures. ΔG° values decreased by 118%, 185% and 7.2% as the temperature increased from 25 to 45°C for the three metals, respectively (Fig. 9). This means that Cd had a high sensitivity to temperature change, while Hg was slightly affected. It was reported that the higher the reaction temperature, the more negative the value of ΔG° will be, indicating high reaction and more favourability at high temperatures (Saha & Chowdhury, 2011). The negative ΔG° values at different temperatures confirm the endothermic nature of the adsorption process. The values of ΔG° are far below the reported values for chemisorption (80–200 kJ/mole), which reinforced the physio-chemical nature of the adsorption process (Saha & Chowdhury, 2011).

The calculated values of the activated energy (Ea) were 18.54, 99.36 and 31.0 kJ/mole for As, Cd and Hg, respectively. It was reported that the positive value of Ea indicates the endothermic and spontaneous nature of the adsorption process, which supported previous results obtained. The values of the sticking probability (S*) are close to zero for As, Cd and Hg ($2.3x10^{-7}$, $1.5x10^{-8}$ and $2x10^{-4}$), indicating high sticking of the metals on the FeN surface.

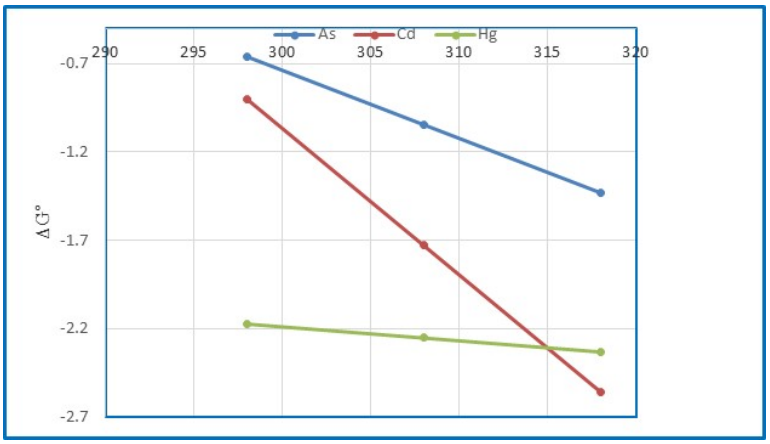

Figure (9): Relationship between temperature and ΔGo

CONCLUSION

Nano-technology has proven to be successful for many engineering applications and water treatment is one of them. In this research, FeN was synthesized by the chemical-precipitation approach and was used for the removal of As, Cd and Hg. The obtained results showed a high removal efficiency of Hg, Cd and As up to 91, 86 and 84% by using FeN and up to 68, 74 and 46% by using FeN-S for the considered metals, respectively. The effects of different operational parameters, such as temperature, pH, mixing time, adsorbent dosage and initial concentration of metal, were investigated and it was found that a pH of 7 provided the optimum removal efficiency for AS and Hg at a mixing time of 120 minutes with an initial concentration of 50ppm and an FeN dose of 0.04. Single adsorption of one metal showed a higher removal efficiency than ternary metals' adsorption. The removal efficiency increased as the adsorbent dosage and temperature increased and decreased as the initial concentrations of metals increased. The results found that in the case of ternary metals, the adsorption process may follow different isotherm models (Langmuir and Freundlich) and the metal ions can be adsorbed on a monolayer (As, Hg) or multi-layers (Cd), while in the case of single scenario, all metals followed Langmuir isotherm model. Thermo-dynamic studies found that the adsorption process is endothermic in nature and is favourable at high temperatures. The kinetic study indicated that the adsorption process for all metals follow to the 2nd-order model.

Acknowledgements

The author is grateful to the Deanship of Scientific Research at Al-Balqa Applied University (BAU) for the support provided during this research program.

Data Availability Statement

The datasets generated and/or analyzed during the current study are available and can be obtained from the corresponding author upon reasonable request.

Conflict of Interest

The author declares that he has no conflict of interest.

REFERENCES

Ahiduzzaman Mohamed, Abul K.M., and Sadrul Islam. (2016). "Evaluation of characteristics of activated carbon from rice husk impregnated with zinc chloride and phosphoric acid". American Journal of Physical Chemistry, 5 (5), 94-98.

Al Hamouz, Othman, Charles, S., and Ali Shaikh, A. (2013). "Removal of zinc and cadmium ions using a cross-linked polyaminophosphonate". Journal of Macro-molecular Science, Part A: Pure and Applied Chemistry, 50 (4), 375-384.

Aljarrah, M.T., Mohammad, S., Al-Harahsheh, M., and Mayyas, Muna Alrebaki. (2018). "*In situ* synthesis of quaternary ammonium on silica-coated magnetic nano-particles and its application for the removal of uranium (VI) from aqueous media". Journal of Environmental Chemical Engineering, 6 (5), 5662-5669.

Alzboon, Kamel. (2017). "Phosphate removal by activated carbon–silica nano-particles composite, kaolin and olive cake". Environment Development and Sustainability, 20 (6), 2707-2724.

AlZboon, Kamel K. (2020). "Impact of olive-cake combustion on ambient air quality using AERMOD model". Indian Journal of Engineering, 17 (48).

Alzboon, Kamel, and Mohammad S. Al-Harahsheh. (2019). "Adsorption of uranium on natural and thermally activated zeolitic tuff: Kinetic, thermo-dynamic and isotherm studies". International Journal of Environment and Waste Management, 24 (1), 21-38.

Alzboon, Kamel K., Bashar, M. Al-Smadi, and Sajedh Al-Khawaldh. (2016). "Natural volcanic tuff-based geopolymer for Zn removal: Adsorption isotherm, kinetic and thermo-dynamic study". Water, Air & Soil Pollution, 227 (7), 227-248.

Alzoubi, F.Y., Al-Zou'by, J.Y., Aljarrah, I.A. et al. (2021). "Physico-chemical characteristics of silver nano-particles: Influence of carbonate alkalinity". Nano-technol. Environ. Eng., 6, 68. https://doi.org/10.1007/s41204-021-00162-9.

Anjaneyulu, U., Priyadarshini, B., and Vijayalakshmi, U. (2018). "Preparation of Ag-doped hydroxyapatite-Fe_3O_4-chitosan composites: *In-vitro* bio-compatibility study on MG-63 cells for orthopedic applications". Advanced Science Letters, 24 (8), 5901-5906.

Bany Yaseen, Ibrahim A., and Zayed Al-Hawari. (2015). "Assessment of heavy-metal pollution of surface sediments in Wadi Shu'ayb, Jordan". Jordan Journal of Civil Engineering, 9 (3), 303-313.

Bertolucci, E. et al. (2015). "Chemical and magnetic properties' characterization of magnetic nano-particles". IEEE International Instrumentation and Measurement Technology Conference (I2MTC) Proceedings, 1492-1496. doi: 10.1109/I2MTC.2015.7151498.

Crini, G. (2005). "Recent developments in polysaccharide-based materials used as adsorbents in wastewater treatment". Progress in Polymer Science, 30 (1), 38-70.

Dada, A.O., Olalekan, A.P., Olatunya, A.M., and Dada, O. (2012). "Langmuir, Freundlich, Temkin and Dubinin–Radushkevich isotherm studies of equilibrium sorption of Zn^{2+} onto phosphoric acid-modified rice husk". Journal of Applied Chemistry, 3 (2), 38-45.

Dargahi, Abdollah, Hafez Golestanifar, Parviz Darvishi, Amir Karami, Syed Hadi Hasan, Ali Poormohammadi, and Alireza Behzadnia. (2016). "An investigation and comparison of removing heavy metals (lead and chromium) from aqueous solutions using magnesium oxide nano-particles". Pol. J. Environ. Stud., 25 (2), 557-562.

Dias, Mariana, João Pinto, Bruno Henriques, Paula Figueira, Elaine Fabre, Daniela Tavares, Carlos Vale, and Eduarda Pereira. (2021). "Nutshells as efficient bio-sorbents to remove cadmium, lead and mercury from contaminated solutions". Int. J. Environ. Res. Public Health, 18 (4), 1580. https://doi.org/10.3390/ijerph18041580

Donat, R., Akdogan, A., Erdem, E., and Cetisli, H. (2005). "Thermo-dynamics of Pb^{2+} and Ni^{2+} adsorption onto natural bentonite from aqueous solutions". Journal of Colloid and Interface Science, 286 (1), 43-52.

Elouear, Z., Bouzid, J., Boujelben, N., Feki, M., Jamoussi, F., and Montiel, A. (2008). "Heavy-metal removal from aqueous solutions by activated phosphate rock". Journal of Hazardous Materials, 156 (1-3), 412-420.

Fato Fato Patrice, Da-Wei Li, Li-Jun Zhao, Kaipei Qiu, and Yi-Tao Long. (2019). "Simultaneous removal of multiple heavy-metal ions from river water using ultrafine meso-porous magnetite nano-particles". ACS Omega, 4 (4), 7543-7549.

Gayatri, Y., Shailaja Raj, M., and Sreedhar, B. (2018). "Characterization of magnetite nano-particles and their role in lead adsorption". International Journal of Scientific and Research Publications, 8 (10), 242-247.

Giraldo, L., Erto, A., and Moreno-Piraján, J.C. (2013). "Magnetite nano-particles for removal of heavy metals from aqueous solutions: Synthesis and characterization". Adsorption, 19 (2-4), 465-474.

Goel Jyotsna, Krishna Kadirvelu, and Chitra Rajagopal. (2004). "Competitive sorption of Cu(II), Pb(II) and Hg(II) ions from aqueous solution using coconut shell-based activated carbon". Adsorption Science & Technology, 22 (3), 257-273.

Han Young-Soo, Averr H. Demond, and Kim F. Haves (2013). "Impact of dissolved silica on arsenite removal by nano-particulate FeS and FeS-coated sand". Chemosphere, 92 (4), 477-481.

Jaishankar, Monisha, Tenzin Tseten, Naresh Anbalagan, Blessy B. Mathew, and Krishnamurthy N. Beeregowda. (2014). "Toxicity, mechanism and health effects of some heavy metals". Interdiscip. Toxicol., 7 (2), 60-72.

Khaled Abbas Abdou, Asmaa Nady Mohammed, Walaa Abd El Rahman Moselhy, and Ahmed Ali Farghali. (2018). "Assessment of modified rice husk and sawdust as bio-adsorbents for heavy-metal removal using nano-particles in fish farm". Asian Journal of Animal and Veterinary Advances, 13 (2), 180-188.

Lui Qing, Fang Li, Hao Lu, Man Li, Jing Liu, Shuangling Zhang, Qingjie Sun, and Liu Lin Xiong. (2018). "Enhanced dispersion stability and heavy-metal ion adsorption capability of oxidized starch nano-particles". Food Chemistry, 242 (1), 256-263.

Malega Ferni, Putu Tedy Indrayana, and Edi Suharyadi. (2018). "Synthesis and characterization of the micro-structure and functional group bond of Fe_3O_4 nano-particles from natural iron sand in Tobelo North Halmahera". Jurnal Ilmiah Pendidikan Fisika Al-Biruni, 7 (2), 13-22.

Manyangadzea, M., Chikuruwob, N.H.M., Narsaiahc, T.B., Chakrad, C.S., Radhakumarie, M., and Danha, G. (2020). "Enhancing adsorption capacity of nano-adsorbents *via* surface modification: A review". South African Journal of Chemical Engineering, 31 (2020), 25-32.

Meng Cheng, Wang Zhikun, Lv Qiang, Li Chunling, Sun Shuangqing, and Hu Songqing. (2018). "Preparation of amino-functionalized Fe3O4@$mSiO_2$ core-shell magnetic nano-particles and their application for aqueous Fe^{3+} removal". Journal of Hazardous Materials, 341 (5), 198-206.

Peng Yuan, Fana Mingde, Yanga Dan, He Hongping, Liua Dong, Yuanc Aihua, Zhu JianXi, and Chen TianHu. (2009). "Montmorillonite-supported magnetite nano-particles for the removal of hexavalent chromium Cr(VI) from aqueous solutions". Journal of Hazardous Materials, 166 (2-3), 821-829.

Roto, Roto. (2018). "Surface modification of Fe_3O_4 as magnetic adsorbents for recovery of precious metals". Advanced Surface Engineering Research (2018). DOI: 10.5772/intechopen.79586.

Saha, P., and Chowdhury, S. (2011). "Insight into adsorption thermo-dynamics". Thermo-dynamics, 34 (2011), 349-364.

Singh, S., Barick, K.C., and Bahadur, D. (2011). "Surface-engineered magnetic nano-particles for removal of toxic-metal ions and bacterial pathogens". Journal of Hazardous Materials, 192 (2011), 1539-1547.

Sismanoglu, T., Ercag, A., Pura, S., and Ercag, E. (2004). "Kinetics and isotherms of dazomet adsorption onto natural adsorbents". J. Braz. Chem. Soc., 15 (5), 669-675.

Sobhanardakani, Soheil, Raziyeh Zandipak, Arash Javanshir-Khoei, Seyed Mehdi Hosseini, Mehran Moslemi, and Parisa Delfieh. (2015). "Removal of Hg (II) and Cd (II) ions from aqueous solution using chitosan: Kinetics and equilibrium studies". Iranian Journal of Health Sciences, 3 (2), 21-30.

Vorokh, A.S. (2018). "Scherrer formula: Estimation of error in determining small nano-particle size". Nano-systems: Physics, Chemistry, Mathematics, 9 (3), 364-369.

Xiaotao Zhang, Yinan Hao, Ximing Wang, Zhangjing Chen, and Chun Li (2016). "Competitive adsorption of cadmium(ii) and mercury(ii) ions from aqueous solutions by activated carbon from xanthoceras sorbifolia bunge hull". Journal of Chemistry, Article ID 4326351, 10 pages. https://doi.org/10.1155/2016/4326351

Yantasee Wassana, Cynthia L. Warner, Thanapon Sangvanich, R. Shane Addleman, Timothy G. Carter, Robert J. Wiacek, Glen E. Fryxell, Charles Timchalk, and Marvin G. Warner. (2007). "Removal of heavy metals from aqueous systems with thiol-functionalized superparamagnetic nano-particles". Environmental Science and Technology, 41 (14), 5114-5119.